PAPER

Germanium-based nearly hyperuniform nanoarchitectures by ion beam impact

Physica Scripta

PAPER

Germanium-based nearly hyperuniform nanoarchitectures by ion beam impact

RECEIVED
21 April 2023

REVISED
1 September 2023

ACCEPTED FOR PUBLICATION
15 September 2023

PUBLISHED
18 October 2023

Jean-Benoit Claude[1], **Mohammed Bouabdellaoui**[2], **Mario Khoury**[2], **Jerome Wenger**[1], **Monica Bollani**[3], **Marco Salvalaglio**[4,5] **and Marco Abbarchi**[2,6,*]

[1] Aix Marseille Univ, CNRS, Centrale Marseille, Institut Fresnel, 13013 Marseille, France
[2] Aix Marseille Univ, Université de Toulon, CNRS, IM2NP, Marseille, France
[3] Istituto di Fotonica e Nanotecnologie-Consiglio Nazionale delle Ricerche, Laboratory for Nanostructure Epitaxy and Spintronics on Silicon, Via Anzani 42, 22100 Como, Italy
[4] Institute of Scientific Computing, TU Dresden, 01062 Dresden, Germany
[5] Dresden Center for Computational Materials Science (DCMS), TU Dresden, 01062 Dresden, Germany
[6] Solnil, 95 Rue de la République, Marseille 13002, France
[*] Author to whom any correspondence should be addressed.

E-mail: marco.abbarchi@im2np.fr

Keywords: disordered hyperuniform, correlated disorder, minkowski functionals, nanofabrication, Germanium on insulator

Supplementary material for this article is available online

Abstract

We address the fabrication of nano-architectures by impacting thin layers of amorphous Ge deposited on SiO_2 with a Ga^+ ion beam and investigate the structural and optical properties of the resulting patterns. By adjusting beam current and scanning parameters, different classes of nano-architectures can be formed, from elongated and periodic structures to disordered ones with a footprint of a few tens of nm. The latter disordered case features a significant suppression of large length scale fluctuations that are conventionally observed in ordered systems and exhibits a nearly hyperuniform character, as shown by the analysis of the spectral density at small wave vectors. It deviates from conventional random fields as accounted for by the analysis of Minkowski functionals. A proof of concept for potential applications is given by showing peculiar reflection properties of the resulting nano-structured films that exhibit colorization and enhanced light absorption with respect to the flat Ge layer counterpart (up to one order of magnitude at some wavelength). This fabrication method for disordered hyperuniform structures does not depend on the beam size. Being ion beam technology widely adopted in semiconductor foundries over 200 mm wafers, our work provides a viable pathway for obtaining disordered, nearly-hyperuniform materials by self-assembly with a footprint of tens of nanometers for electronic and photonic devices, energy storage and sensing.

1. Introduction

Hyperuniform (HU) systems are characterized by the suppression of large-wavelength density fluctuations owing to a hidden order which is not apparent on short lengthscales [1, 2]. Systems possessing long-range translational and orientational order, e.g. crystalline structures and periodic fields, represent trivial cases of HU structures. More interestingly, a HU character may be present in disordered systems with partial or full suppression of density fluctuations for small wavevectors (similarly to crystalline solids) and isotropic behaviors with respect to spatial directions (as for liquids). These features are well described for point patterns by the structure factor $S(\mathbf{k})$ with $\mathbf{k}$ the wavevector. Ideal HU characters corresponds to have a scaling $S(\mathbf{k}) \sim |\mathbf{k}|^{\alpha}$ for $|\mathbf{k}| \to 0$ and $\alpha > 0$. Generalizations have been proposed to account for such a property in systems as, e.g. heterogeneous media as well as scalar and vector fields [2–4]. In experimental settings, quantification of the HU character (how close a system is to the ideal HU case) is typically considered through the metrics $H = S(|\mathbf{k}| \to 0)/\max(S(|\mathbf{k}|))$, with condition $H \lesssim 10^{-2}$ and $H \lesssim 10^{-4}$ commonly denoting nearly and effective HU character, respectively [5, 6].

Table 1. List of samples, composition of their layers and FIB scanning conditions. We report the beam energy (keV), angle of incidence (degrees) and scan strategy (individual and multiple, respectively S and M).

Sample	Composition	Buried Oxide	FIB energy	FIB angle	FIB scan
A	50 nm a-Ge/7 nm SOI	2 μm	30 keV	0 deg.	S and M
B	50 nm a-Ge	30 nm	30 keV	0 deg.	M
C	200 nm a-Ge	300 nm	30 keV	0 deg.	M

Materials and architectures possessing a nearly, effective or ideal HU character have gained a lot of interest in recent years. In addition to fundamental physical aspects [2, 7], their importance relies in the novel possibilities in light [8–18] and carrier management with topologically-protected electronic states [19] as well as vortices in superconductors [20]. A crucial aspect consists of finding a proper fabrication method that allows the realization of a HU material, e.g. small enough H, at wavelengths of interest for the targeted applications. Design protocols for the realization of HU patterns have been developed [11]. They have usually been combined with top-down approaches. Although powerful, see e.g. [16, 17, 21], such approaches usually show poor scalability. This becomes crucial for patterns meant for large-area applications with features on the nanometer scale, such as metals and nanostructured semiconductor films for photonics applications.

Devising scalable approaches for the fabrication of HU materials featuring nanostructured architectures represents then an important goal. Self-assembly paradigms or hybrid bottom-up/top-down approaches have been exploited for decades to obtain nano- and micro-structures from film-like settings [22–24]. Self-assembly based on spinodal-like, solid-state dewetting has also recently proved successful for the fabrication of effectively HU, SiGe-based nano-architectures with a footprint of about 100 nm [25]. Such an approach can be scaled-up to large surfaces [26]. Moreover, soft nano-imprint lithography of sol-gel materials (such as silica and titania) was also exploited to fabricate nearly-HU metasurfaces using dewetted micro-and nano-architectures as hard masters [18]. Table 1.

A remarkable example of self-assembly in crystalline and amorphous Ge semiconductor thin-films consists of the impact of ion beams, widely investigated both from experimental [27–30] and theoretical point of views [31–33]. Formation of periodic, ordered [34, 35] and disordered nano-architectures with this approach has been largely addressed so far, and we thus refer the reader to the existing literature [28, 31, 36, 37]. Central aspects of this approach are its versatility, as the features can be tuned by varying the ion beam parameters (e.g. ion species, energy, and dose [30, 38], incidence angle [39], sample temperature [27] and stochiometry [40]) and processable surface that can reach 200mm wafers. These structures can also extend over several hundreds of nanometers in depth, below the surface, resulting in actual three-dimensional, porous nanoarchitectures with an average cavity radius as small as a few tens of nm [40, 41].

Here we report on Ge-based nano-structures obtained by the impact of a high-energy, Ga^+ ion beam on Ge layers deposited on silicon on insulator (SOI) resulting in ordered and disordered nano-architectures and characterize their morphological features. We show the formation of strongly anisotropic and wavy structures as well as isotropic disordered ones, obtained by adjusting ion current, supplied dose, and scanning parameters. We focus then on the isotropic disordered pattern, being the main target of this study, and we discuss its features. The nearly-HU character of the disordered structures is assessed through the analysis of their *spectral density* accounting for the formation of Ge-based nearly-HU nano-architectures having a record footprint of about 40 nm. The analysis of the Minkowski functionals of the patterns further assesses their deviations from a (Gaussian) random field and supports the presence of correlations in the patterns. A proof of concept for potential applications is then given in section 4, showing peculiar reflection properties of the resulting nanostructured film. For the sake of readibility, we report in the main text the main evidence and results, while including additional materials in the Supporting Information. Conclusions are summarized in section 5.

2. Results

2.1. Experimental methods

We used several kind of substrates where very similar structures can be obtained. Here, in than main text, we address only three samples, A, B and C described in detail in table 1. On each sample the FIB process has been changed producing many different patterns. However, for all the samples, theions and their energy is kept constant (Ga at 30 keV). For each of them, the FIB dose and scan features are specified in the corresponding figure and in the corresponding text.

a-Ge deposition on SOI is performed as follows: after chemical cleaning (5 seconds in 10% HF solution in H_2O in N_2 atmosphere), amorphous Ge is deposited by molecular beam epitaxy (Riber R32, in ultra-high

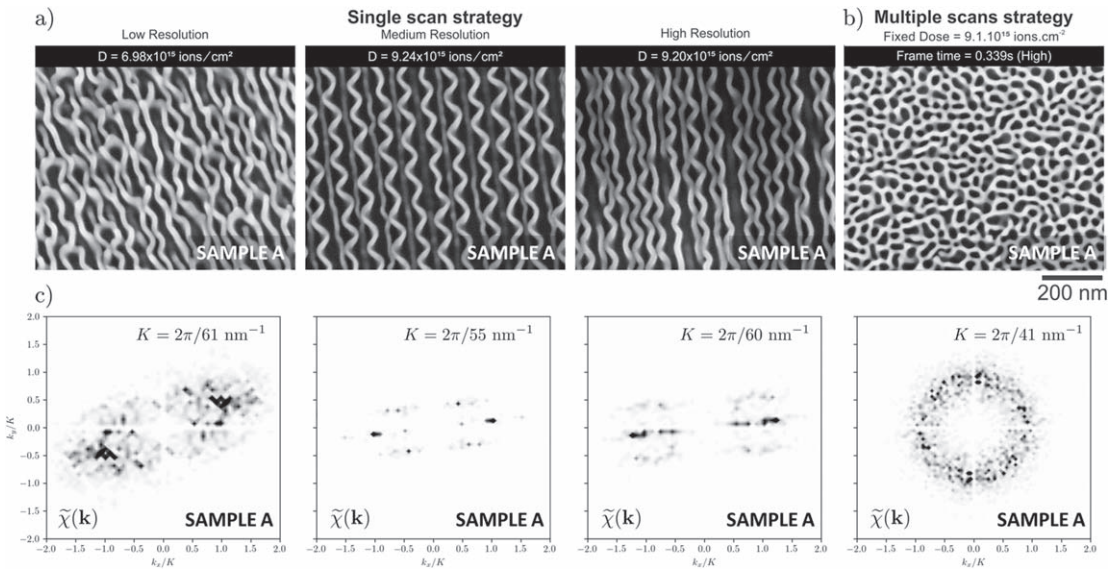

Figure 1. Influence of FIB single scanning mode. Sample A. (a) High-resolution scanning electron microscopy (SEM) images of a Ge layer on silicon on insulator (SOI) processed by FIB with a single scan strategy using low, medium, and high resolution (respectively 256 × 221 pixels, 512 × 442 pixels and 1024 × 884 pixels) with ion beam fluency in the 10^{15} ions cm^{-2} range. (b) SEM image of a Ge layer on SOI processed by FIB with a multiple scan strategy and high resolution. In this condition, high and low resolution exhibit the same final morphology with a nearly-HU character. (c) Spectral density $\widetilde{\chi}(\mathbf{k})$ for the samples illustrated in panels (a) and (b). The white-to-black color scale is saturated at 0.75 max($\widetilde{\chi}(\mathbf{k})$). K corresponds to the wavevector length at which the max($\widetilde{\chi}(\mathbf{k})$) is obtained.

vacuum of $\sim 10^{-10}$ torr, at room temperature and growth rate of 10 Å/min). a-Ge deposition on SiO_2 is performed as on SOI but without chemical cleaning with HF.

We used a dual-beam FEI Strata DB235 with Ga^+ (atomic mass 31 amu) liquid-metal ion source focused ion beam (FIB) and a SFEG source for the scanning electron microscope imaging (SEM). We used ion currents within 15 and 1000 pA at 30 keV. The samples are kept orthogonal to the Ga ion beam. The FIB beam moves horizontally, from the top left part of the window and line-by-line, raster-scans the sample surface, down to the bottom right point.

Monte Carlo simulation of Ga ion range at 30 keV and normal incidence in bulk Ge shows that most of the ions stop within the first 50 nm with a broadening of about 22 nm. This relatively small penetration accounts for the fact that the morphologies observed on Ge samples (bulk and thin films) implanted with Ga obtained for a defined dose and scanning conditions are very similar.

2.2. Pattern formation for single and multiple scans

We now discuss two different scanning conditions: single scans and multiple scans. For both cases we compare patterns obtained with similar ions doses.

For single scans (sample A, figure 1(a)), the ion beam resolution is set to low (256 × 221 pixels), medium (512 × 442 pixels), and high (1024 × 884). At 50000× magnification (used for the milling process), the field of view has a side of 6080 nm. Thus, each pixel is respectively separated by 24, 12, and 6 nm for low, medium, and high resolution. The ion current was fixed at 30 pA, corresponding to a beam diameter of about 15 nm. Thus, only low-resolution modes do not result in a beam overlapping from one point to the other. As shown in figure 1(a), different resolution impacts the final morphology with different features. For the sake of thoroughness we mention that in these FIB conditions using thin film of a-Ge on SOI or bulk c-Ge as substrate does not play a role owing to the high ion dose in use.

The disordered hyperuniform patterns shown in this work can be obtained in a rather broad range of FIB parameters. Here, among all the results, we display only those obtained in similar conditions (e.g. ion dose about 10^{16} ion/cm^2 or larger, figures 1, 2 and 3(b)). Only in one case we display a lower dose of about 10^{15} ion/cm^2 in order to show the early stages of the pattern formation (figure 4(a)). Other conditions (e.g. number of FIB scans, frame time are provided in the Supplementary Information).

Pattern formation by ion beam impact is a complex phenomenon [42] and its analysis goes beyond the scope of this paper. Here we refer the reader to the theory of pattern formation in references [31, 36, 37, 39, 42–44] where the role of different parameters (e.g. beam energy, ion mass, angle of incidence, mass redistribution and curvature-depending sputtering) are considered. When the ion beam and the processed materials are not composed of the same element, as in our case, binary compounds theory should be taken into account as

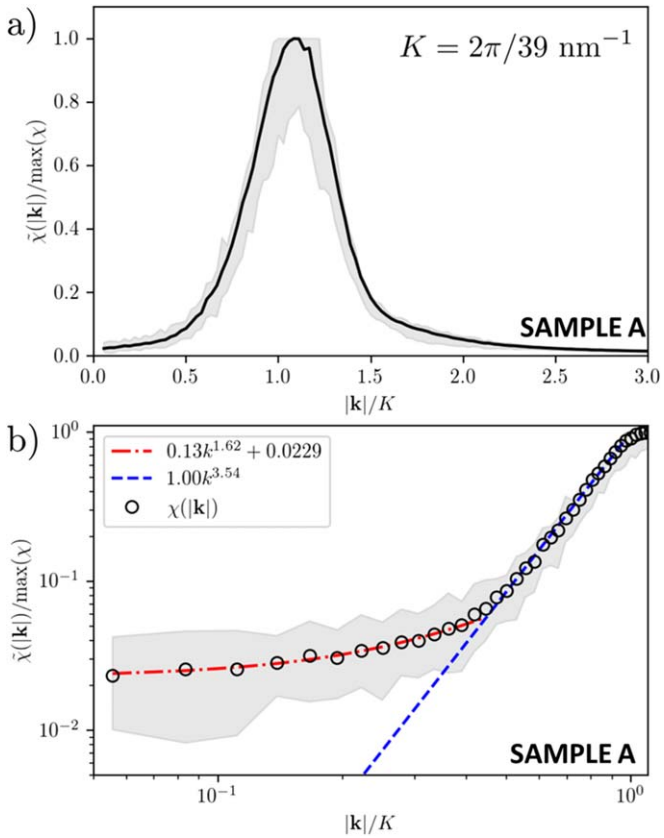

Figure 2. Spectral density and assessment of the nearly-HU character. Sample A. (a) Radial distribution of the normalized spectral density for sample A averaged over 50 images of different location irradiate with the same dose of 8×10^{16} ions cm^{-2} (see the Supplementary Information for a composition of all the images). The shaded grey areas displays the variability of the spectral density measured over all the 50 repetitions of the pattern. (b) Log-log plot for the curve in panel (a) focusing on the region $|\mathbf{k}|/K \leqslant 1$ and showing the decay for $|\mathbf{k}| \to 0$.

showcased in reference [44] and more specifically for Ge in reference [39]. In this latter case that we consider in our work, other phenomena are expected to play a major role in patter formation, such as vacancy clustering [29, 30], ion-induced melting of the a-Ge layer [45] and swelling by atom displacement [41, 43].

Different ions (e.g. Ar^+, Xe^+, Kr^+) can produce wavy structures on Si and Ge wafers [46–48]. However, the porous structures observed here are very specific of Ge. It is also worth mentioning that similar patterns can be obtained in metals under strong laser illumination [49] and ion beam impact in [50, 51].

3. Pattern analysis

Global features of the patterns as in figure 1 can be analyzed by looking at their spectral density $\tilde{\chi}(\mathbf{k})$. It provides the generalization for the information conveyed by the structure factor $S(\mathbf{k})$ for point patterns [2]. The SEM images collected for the structures (c.f. figure 1 for sample A) well resolve the region occupied by the solid phase with respect to the surrounding vacuum. Therefore we consider the spectral density $\tilde{\chi}(\mathbf{k})$ for a two-phase (solid-vacuum) system [3]. It is based on an indicator function:

$$\mathcal{I}^{(s)}(\mathbf{r}) = \begin{cases} 1, & \mathbf{r} \in \mathcal{V}_s, \\ 0, & \mathbf{r} \notin \mathcal{V}_s, \end{cases} \tag{1}$$

with $\mathbf{r} \in \Omega$ the spatial coordinates and $\mathcal{V}_s$ the region with grey-scale values above a given threshold. $\tilde{\chi}(\mathbf{k})$ then corresponds to the Fourier transform of the autocovariance function [3, 52]:

$$\chi(\mathbf{r}) = \mathcal{S}_2^{(s)}(\mathbf{r}) - (\phi^{(s)})^2, \tag{2}$$

with

$$\mathcal{S}_2^{(s)}(\mathbf{r}) = \langle \mathcal{I}^{(s)}(\mathbf{r}')\mathcal{I}^{(s)}(\mathbf{r}' + \mathbf{r}) \rangle, \tag{3}$$

the two-points autocorrelation function and $\phi^{(s)} = \langle \mathcal{I}^{(s)}(\mathbf{r}') \rangle$ the volume fraction of the solid phase. The spectral density can be computed directly as [52]:

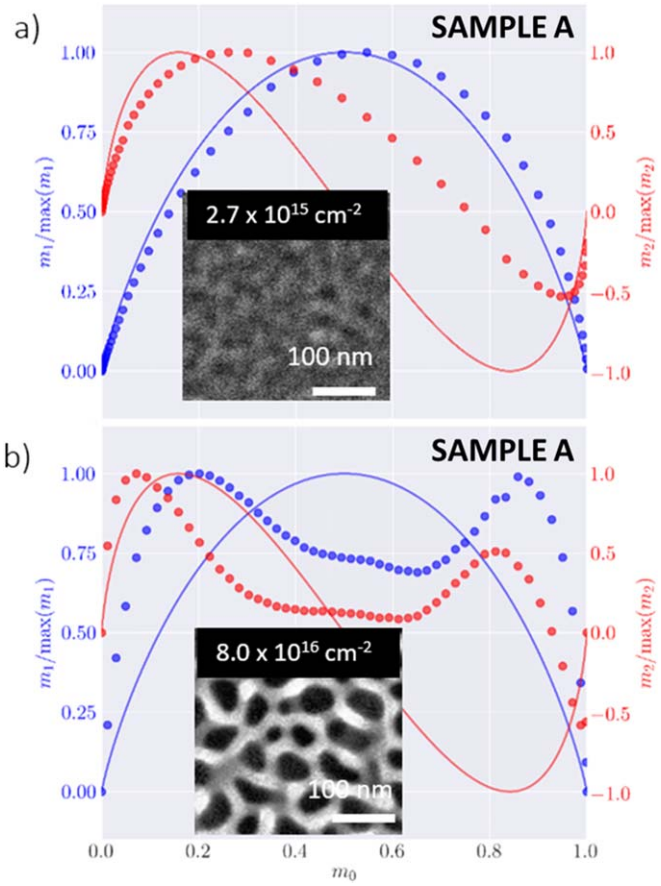

Figure 3. Disorder and correlations of spontaneous patterns. Sample A. (a) Minkowski functionals analysis $m_{1,2}(m_0)$ for sample A (50 nm thick Ge layer atop 7 nm SOI) exposed to multiple scans and high resolution with an overall dose of 2.7×10^{15} ions cm^{-2}. Continuous lines represent the trend of $m_{1,2}(m_0)$ for a Gaussian random field. The insets show SEM micrographs with details of the sample's surface. (b) Same as (a) for 8.02×10^{15} ions cm^{-2} dose.

$$\widetilde{\chi}(\mathbf{k}) = \frac{1}{|\Omega|}|\mathcal{F}[\mathcal{I}^{(s)}(\mathbf{r}) - \phi_i]|^2 \tag{4}$$

with $\mathcal{F}$ the Fourier transform and $|\Omega|$ the area of the images. The decay of $\widetilde{\chi}(\mathbf{k})$ for $\mathbf{k} \to 0$ conveys similar information to $S(|\mathbf{k}|)$ [2, 3].[7]

The spectral density for the patterns obtained on sample A in figure 1(a) is shown in the first three panels of figure 1(c). The structures exhibit anisotropic arrangements with marked periodicity. The characteristic frequency K (where the peak of $\widetilde{\chi}(\mathbf{k})$ is observed) is reported in the figures and points to characteristic length scales $2\pi/K$. For low resolution, the structures present a higher degree of disorder which is then reduced for larger resolution. The patterns are also found to exhibit slightly different predominant orientations $>83^\circ$ tilt with respect to the scan direction, medium resolution 75°–83°, and low resolution 61°–70°. As expected for (partially-) ordered structures, the corresponding spectral density show an exclusion zone at small wavevectors. This analysis shows that, depending on how the ions are supplied, different anisotropic structures can be obtained with tuneable disorder.

A behavior similar to the patterns illustrated above in terms of suppression of correlations at large wavelength (with an exclusion zone at small wavevectors), has been obtained through a multiple scans strategy, using an overall dose of 9.1×10^{15} ions cm^{-2} (figure 1(b)). However, this time the final structure features a spectral density $\widetilde{\chi}(\mathbf{k})$ with isotropic angular distribution (last panel in figure 1(c) for sample A) that corresponds to a disordered and uniform distribution of objects. Exploring the three different resolution configurations always provides the same morphology featuring connected and disordered structures, even when using an overall dose comparable to that of a single scan (see Supplementary Information).

Beyond raster scans with a small spot (as shown in figure 1(b)), sample A), disordered, porous a-Ge can be obtained also by ion impact on a single large spot (see the Supplementary Information). This demonstrates that

[7] Interestingly, results similar to the one reported in the following can be obtained by sampling the solid phase with randomly distributed points and computed $S(\mathbf{k})$.

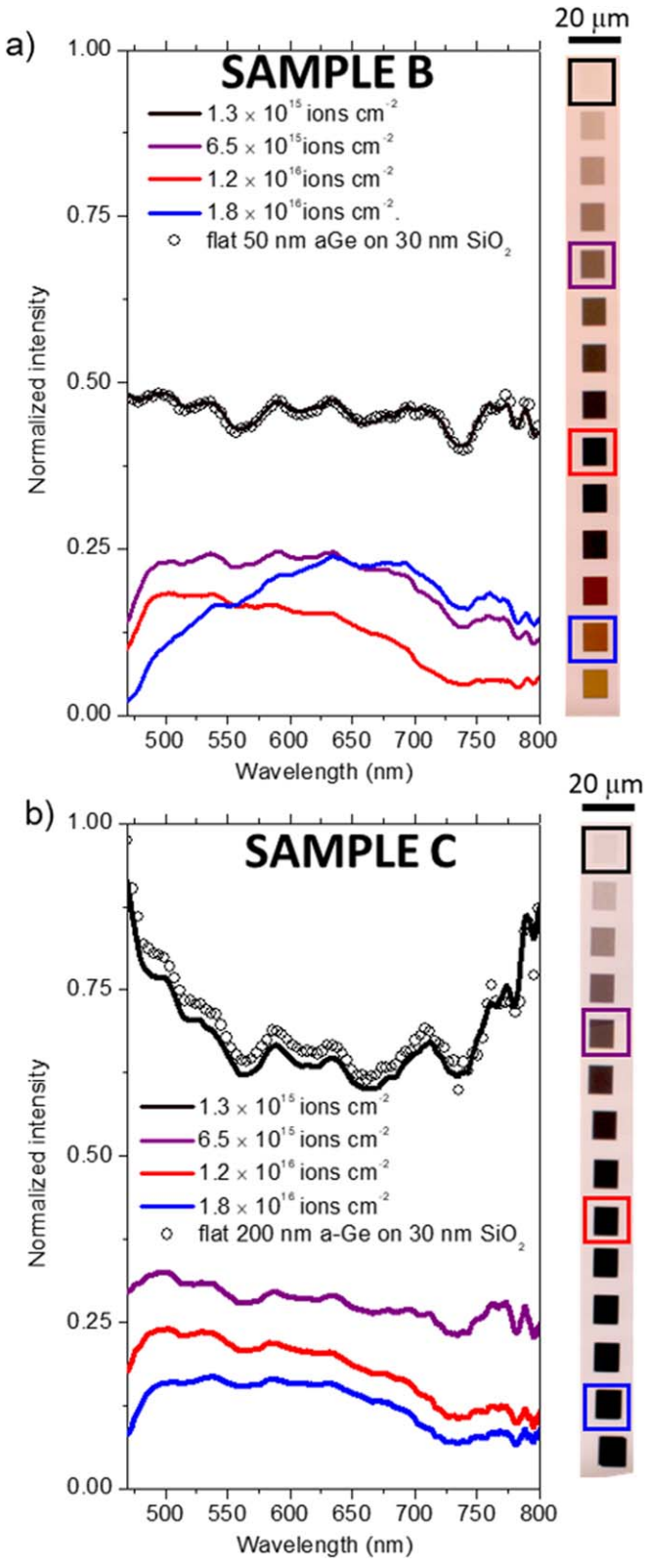

Figure 4. Light reflection from porous a-Ge. (a) Reflection from sample B (50 nm a-Ge on 30 nm thick SiO_2) normalized by the white tungsten lamp used for illumination. Open symbols correspond to flat sample before FIB processing, whereas continuous lines are impacted areas with a multiple scan and high resolution approach. The overall doses on the samples are reported in the legend. Spectra are collected in bright field illumination with a 100×magnification objective lens, numerical aperture 0.9 (collection angle about ±64 degrees, lateral, resolution ~6 μm. Right inset: from top to bottom, bright-field images of the impacted areas with doses ranging from 0 to 2.3 × 10^{16} ions cm^{-2}. The areas highlighted with squares are those selected for spectroscopy. (b) Same as (a) for sample C (200 nm thick a-Ge on 30 nm SiO_2).

the fabrication process can be scaled to much larger surfaces as it does not require a high lateral resolution. Nonetheless, the possibility of creating these patterns over small and well-defined areas may allow to integrate them within other devices.

We now further asses the disorder found in the case of uniform structures. We provide a quantitative assessment of the HU character of the uniform and disordered pattern in figure 1(b) and address their scalability by analyzing 50 separate images in different points on sample A (see a collage in the Supplementary Information). In figure 2, we report the normalized radial distribution of $\widetilde{\chi}(\mathbf{k})$ averaged over all the analyzed images. Grey areas show the range of variability of the results across the different images. Figure 2(a) shows a marked peak at about 0.16 nm^{-1} corresponding to a characteristic length-scale of ~39 nm (±4 nm). We observe a decay of $\widetilde{\chi}(\mathbf{k})$ toward zero, sampled up to the limits of the analyzed window, well approximated by $|\mathbf{k}|^{\alpha}$ with $\alpha \approx 3.5$ close to $|\mathbf{k}|/K = 1$ (see log-log plot in figure 2(b)).

An extrapolation of $\widetilde{\chi}(0)$ through fitting allows to estimate a H-metric value of $H \approx 2 \cdot 10^{-2}$ for the averaged $\widetilde{\chi}(\mathbf{k})$, and within a range $H \in [8 \cdot 10^{-3} - 3 \cdot 10^{-2}]$ among the analysed samples. This value is compatible with a nearly-HU character [5, 6] similarly to other systems where correlations and HU character emerge spontaneously [53, 54].

The features of the disordered structures can be further analyzed by Minkowski functionals. These tools allow for describing the topological features of patterns [25, 55, 56]. Importantly, they can be used as a test to determine the deviation to Gaussian random fields. These deviations can be related to underlying short-range interactions and non-linear dynamics [57, 58]. It is worth mentioning that Gaussian random fields may be ideally constructed to be hyperuniform [4]. This analysis, therefore, complements the quantification of the hyperuniform character, namely the results reported in figure 2 for sample A, with further robust insights on the mechanism underlying the pattern formation (see, e.g. the assessment of spinodal-like structures in [25]).

We plot averaged Minkowski functionals $m_i(\bar{\rho}) = (1/|\Omega|)M_i(\mathcal{B}_{\bar{\rho}})$ with M_i the non-averaged functionals and $|\Omega|$ the total size of the image. $\mathcal{B}_{\bar{\rho}}$ is an indicator function such that $\mathcal{B}_{\bar{\rho}} = 1$ for $\rho > \bar{\rho}$ and $\mathcal{B}_{\bar{\rho}} = 0$ for $\rho < \bar{\rho}$ with $\rho \in [0, 255]$ the grey-scale value in a given position (pixel) and $\bar{\rho}$ a threshold that is varied from the maximum and minimum value of ρ [25, 57] (figure 3, sample A). $m_0(\bar{\rho})$ is the fraction of $|\Omega|$ occupied by the non-zero region in $\mathcal{B}_{\bar{\rho}}$,as $M_0(\mathcal{B}_{\bar{\rho}})$ represents the area of $\mathcal{B}_{\bar{\rho}} = 1$. $m_1(\rho)$ is the average of the boundary length U between the areas where $\mathcal{B}_{\bar{\rho}} = 1$ and $\mathcal{B}_{\bar{\rho}} = 0$, as $U = 2\pi M_1(\mathcal{B}_{\bar{\rho}})$. $m_2(\rho)$ is the averaged Euler characteristic χ, as $\chi = \pi M_2(\mathcal{B}_{\bar{\rho}})$. With this method, the results are independent of image saturation and contrast [25, 57].

$m_{1,2}(m_0)$ assess the deviation from a random field (solid lines in figures 4(a) and (b), sample A) and eventual non-linearity [31, 59] of the underlying pattern formation dynamics [57]. We observe significant deviations from a Gaussian random field of $m_1(m_0)$ and $m_2(m_0)$ for porous Ge irradiated with 8.0×10^{16} ions cm^{-2} (figure 4(b)), which increase with increasing the dose. Other FIB settings (e.g. lower beam energy), as in T. Bottger *et al* [30] result in disordered structures very close to a Gaussian random field (see the Supplementary Information).

Despite the fact that the disordered patterns reported in this paper have already been shown in the past in many works and that it is well known that the dynamics underlying the formation of these patterns is non-linear, a complete analysis of the topology using Minkowski functionals had not yet been done [60]. As previously reported for hyperuniform patterns obtained by spinodal-like dewetting of metals [61], polymers [58] and semiconductors [25], the Minkowski functionals catch and quantify the deviations of a disordered pattern from a Gaussian random field accounting for the presence of non-linearity in the underlying phenomenon. In our case (and also comparing our results with the literature where beams with lower energy were used [30], see the Supplementary Information), it is clear that this theoretical framework accounts for the progressively-increasing importance of non-linear effects in the pattern formation dynamics.

4. Optical properties

Finally, we address the changes in light reflection from the impacted areas featuring a nearly-HU character for sample B and C. A spectroscopic characterization of light reflection performed in bright-field illumination reveals strong changes of optical response in the processed areas with respect to the flat counterpart (figure 4). SEM images of the impacted areas for the patterns investigated by optical spectroscopy for sample B are provided in the Supplementary Information.

The 50 nm thick a-Ge layer deposited atop 30 nm thick SiO_2 (sample B) shows a drastic reduction in the reflected light intensity when impacted with a dose larger than $\sim 5 \times 10^{15}$ cm^{-2} with a multiple scan strategy and high resolution. A minimum in reflection is observed for a dose of 1.2×10^{16}, that is close the value for the onset of the dHU patterns as previously highlighted in figures 1(b) and figure 3(b). For larger doses, exceeding 1.3×10^{16} cm^{-2}, a red colorization appears. From the spectroscopic investigation, we attribute this feature to enhanced absorption at short wavelength, cutting the blue light reflection (up to about 25 times larger than the flat counterpart).

Qualitatively similar results are obtained with a 200 nm thick a-Ge on 30 nm buried oxide (sample C, figure 4(b)). However, in this case, a reduced reflection at short wavelength is not present (the spectra are less structured with respect to the previous case of thin a-Ge). Provided the presence of several layers with different optical

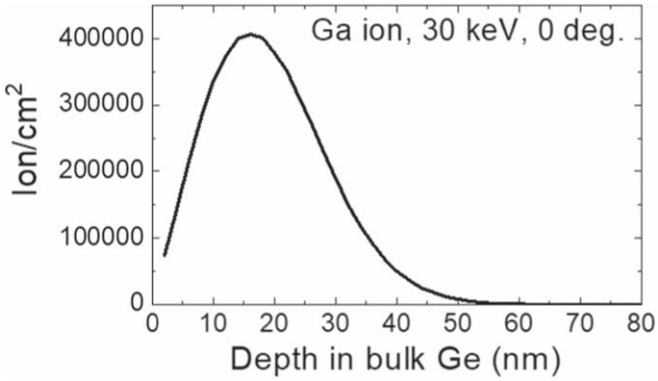

Figure 5. Monte Carlo simulations of ion implant. Ga ion range in bulk Ge calculated with SRIM software. The ion energy is 30 keV and the incidence angle of 0 degrees.

constants, the overall response to illumination (e.g. the color) is also determined by etalon effects and by the disordered network of filaments as also found in similar disordered structures [62, 63].

From Monte Carlo simulations run with SRIM software (figure 5) we understand that for a 50 nm thick a-Ge (as in sample B) the full layer is impacts by the Ga ions. As such, the optical properties of Ge are heavily affected by the implant. For the thicker sample, with a-Ge of 200 nm, the Ga ions stop in the top layer. Thus, beyond the etalon effects that might impact the optical response, Ga ion implant can be also a potential origin of the observed difference between thin and thick a-Ge.

Qualitatively similar results in light reflection were recently reported for porous Ge obtained by ion implant [64] although the nearly-dHU character of the patterns was not reported. In those cases, at visible frequency, a reduction of about a factor of 3 with respect to the flat Ge case was shown, whereas for our patterns an overall reduction up to a factor of 4 (or larger at some wavelength) can be obtained. This improved performances of our devices can be ascribed to a finer tuning of the implant conditions.

The typical back-scattering of light from dHU structures showcases a ring in the far field [15, 18, 65]. However, for structures with such a small footprint as those showed here (K0.16 nm^{-1}, figure 2, sample A) and in reference [64] the scattering in such a cone cannot couple to the far field and stays trapped within the underlying substrate. This can explain the good anti-reflection properties displayed by the textured a-Ge. Thus, despite it is not possible to directly link the optical response of these nearly-dHU structures to their the dHU character our evidence further confirm the relevance of these materials for light trapping as also thoroughly shown in recent reports [15, 65].

5. Conclusions

In conclusion, we showed that impacting a thin layer of Ge with an ion beam results in ordered and disordered structures with a nearly-HU character. Their typical size is the smallest reported so far for analogous HU systems [21, 25, 65]. Provided the possibility to change stochiometry by Si alloying [40], tune the size of the pores by changing ion dose [29, 38] or Ge film thickness [41] and also obtain truly 3D structures [29, 41], this fabrication approach has considerable potential for overcoming the limitations of conventional methods for nanoarchitectures with HU character [66].

Acknowledgments

This research was funded by the EU H2020 FET-OPEN project NARCISO (No. 828 890). J. W. and J.-B. C. acknowledge the European Research Council (ERC, Grant Agreement No. 723 241). We acknowledge the Nanotecmat platform of the IM2NP institute of Marseilles.

Data availability statement

All data that support the findings of this study are included within the article (and any supplementary files).

ORCID iDs

Jean-Benoit Claude https://orcid.org/0000-0001-9618-0576
Jerome Wenger https://orcid.org/0000-0002-2145-5341
Monica Bollani https://orcid.org/0000-0002-0078-5085
Marco Salvalaglio https://orcid.org/0000-0002-4217-0951
Marco Abbarchi https://orcid.org/0000-0002-2760-4766

References

[1] Torquato S and Stillinger F H 2003 Local density fluctuations, hyperuniformity, and order metrics *Phys. Rev.* E **68** 041113
[2] Torquato S 2018 Hyperuniform states of matter *Phys. Rep.* **745** 1
[3] Torquato S 2016 Hyperuniformity and its generalizations *Phys. Rev.* E **94** 022122
[4] Ma Z and Random S 2017 Torquato scalar fields and hyperuniformity *J. Appl. Phys.* **121** 244904
[5] Torquato S, Uche O U and Stillinger F H 2006 Random sequential addition of hard spheres in high euclidean dimensions *Phys. Rev.* E **74** 061308
[6] Kim J and Torquato S 2018 Effect of imperfections on the hyperuniformity of many-body systems *Phys. Rev.* B **97** 054105
[7] Gabrielli A, Joyce M and Labini F S 2002 Glass-like universe: real-space correlation properties of standard cosmological models *Phys. Rev.* D **65** 083523
[8] Froufe-Pérez L S, Engel M, Sáenz J J and Scheffold F 2017 Band gap formation and anderson localization in disordered photonic materials with structural correlations *Proc. Natl. Acad. Sci. U.S.A.* **114** 9570
[9] Zhou W, Cheng Z, Zhu B, Sun X and Tsang H K 2016 Hyperuniform disordered network polarizers *IEEE J. Sel. Top. Quantum Electron.* **22** 288
[10] Yu S, Qiu C-W, Chong Y, Torquato S and Park N 2020 Engineered disorder in photonics *Nat. Rev. Mater.* **1** 226–43
[11] Florescu M, Torquato S and Steinhardt P J 2009 Designer disordered materials with large, complete photonic band gaps *Proc. Natl. Acad. Sci. U.S.A.* **106** 20658
[12] Man W, Florescu M, Williamson E P, He Y, Hashemizad S R, Leung B Y, Liner D R, Torquato S, Chaikin P M and Steinhardt P J 2013 Isotropic band gaps and freeform waveguides observed in hyperuniform disordered photonic solids *Proc. Natl. Acad. Sci. U.S.A.* **110** 15886
[13] Froufe-Pérez L S, Engel M, Damasceno P F, Muller N, Haberko J, Glotzer S C and Scheffold F 2016 Role of short-range order and hyperuniformity in the formation of band gaps in disordered photonic materials *Phys. Rev. Lett.* **117** 053902
[14] Wu B-Y, Sheng X-Q and Hao Y 2017 Effective media properties of hyperuniform disordered composite materials *PLoS One* **12** e0185921
[15] Piechulla P M, Fuhrmann B, Slivina E, Rockstuhl C, Wehrspohn R B and Sprafke A N 2021 Tailored light scattering through hyperuniform disorder in self-organized arrays of high-index nanodisks *Adv. Opt. Mater.* **9** 2100186
[16] Granchi N, Spalding R, Lodde M, Petruzzella M, Otten F W, Fiore A, Intonti F, Sapienza R, Florescu M and Gurioli M 2022 Near-field investigation of luminescent hyperuniform disordered materials *Adv. Opt. Mater.* **10** 2102565
[17] Granchi N, Lodde M, Stokkereit K, Spalding R, van Veldhoven P, Sapienza R, Fiore A, Gurioli M, Florescu M and Intonti F 2023 Near-field imaging of optical nanocavities in hyperuniform disordered materials *Phys. Rev.* B **107** 064204
[18] Chehadi Z, Bouabdellaoui M, Modaresialam M, Bottein T, Salvalaglio M, Bollani M, Grosso D and Abbarchi M 2021 Scalable disordered hyperuniform architectures via nanoimprint lithography of metal oxides *ACS Appl. Mater. Interfaces* **13** 37761
[19] Mitchell N P, Nash L M, Hexner D, Turner A M and Irvine W T 2018 Amorphous topological insulators constructed from random point sets *Nat. Phys.* **14** 380
[20] Rumi G, Sánchez J A, Elías F, Maldonado R C, Puig J, Bolecek N R C, Nieva G, Konczykowski M, Fasano Y and Kolton A B 2019 Hyperuniform vortex patterns at the surface of type-ii superconductors *Phys. Rev. Research* **1** 033057
[21] Castro-Lopez M, Gaio M, Sellers S, Gkantzounis G, Florescu M and Sapienza R 2017 Reciprocal space engineering with hyperuniform gold disordered surfaces *APL Photonics* **2** 061302
[22] Medeiros-Ribeiro G, Bratkovski A M, Kamins T I, Ohlberg D A A and Williams R S 1998 Shape transition of germanium nanocrystals on a silicon (001) surface from pyramids to domes *Science* **279** 353
[23] Ye J and Thompson C V 2011 Templated solid-state dewetting to controllably produce complex patterns *Adv. Mater.* **23** 1567
[24] Naffouti M *et al* 2017 Complex dewetting scenarios of ultrathin silicon films for large-scale nanoarchitectures *Sci. Adv.* **3** eaao1472
[25] Salvalaglio M *et al* 2020 Hyperuniform monocrystalline structures by spinodal solid-state dewetting *Phys. Rev. Lett.* **125** 126101
[26] Benali A *et al* 2020 Flexible photonic devices based on dielectric antennas *J. Phys. Photonics* **2** 015002
[27] Bischoff L, Pilz W and Schmidt B 2011 Amorphous solid foam structures on germanium by heavy ion irradiation *Appl. Phys.* A **104** 1153
[28] Kolíbal M, Matlocha T, Vystavěl T and Šikola T 2011 Low energy focused ion beam milling of silicon and germanium nanostructures *Nanotechnology* **22** 105304
[29] Rudawski N G and Jones K S 2013 Nanostructured germanium prepared via ion beam modification *J. Mater. Res.* **28** 1633
[30] Böttger R, Heinig K-H, Bischoff L, Liedke B and Facsko S 2013 From holes to sponge at irradiated ge surfaces with increasing ion energyan effect of defect kinetics? *Appl. Phys.* A **113** 53
[31] Bradley R M and Harper J M 1988 Theory of ripple topography induced by ion bombardment *J. Vac. Sci. Technol.* **6** 2390
[32] Nord J, Nordlund K and Keinonen J 2002 Amorphization mechanism and defect structures in ion-beam-amorphized Si, Ge, and GaAs *Phys. Rev.* B **65** 165329
[33] Hartmann A K, Kree R and Yasseri T 2009 Simulating discrete models of pattern formation by ion beam sputtering *J. Phys. Cond. Matter* **21** 224015
[34] Wei Q, Zhou X, Joshi B, Chen Y, Li K-D, Wei Q, Sun K and Wang L 2009 Self-assembly of ordered semiconductor nanoholes by ion beam sputtering *Adv. Mater.* **21** 2865
[35] Fritzsche M, Muecklich A and Facsko S 2012 Nanohole pattern formation on germanium induced by focused ion beam and broad beam Ga+ irradiation *Appl. Phys. Lett.* **100** 223108
[36] Cuerno R and Barabási A-L 1995 Dynamic scaling of ion-sputtered surfaces *Phys. Rev. Lett.* **74** 4746

[37] Castro M, Cuerno R, Vázquez L and Gago R 2005 Self-organized ordering of nanostructures produced by ion-beam sputtering *Phys. Rev. Lett.* **94** 016102
[38] Hooda S, Khan S, Satpati B, Stange D, Buca D, Bala M, Pannu C, Kanjilal D and Kabiraj D 2016 Effect of ion beam parameters on engineering of nanoscale voids and their stability under post-growth annealing *Appl. Phys.* A **122** 227
[39] Mollick S A, Ghose D, Shipman P D and Bradley R M 2014 Anomalous patterns and nearly defect-free ripples produced by bombarding silicon and germanium with a beam of gold ions *Appl. Phys. Lett.* **104** 043103
[40] Alkhaldi H, Kremer F, Bierschenk T, Hansen J, Nylandsted-Larsen A, Williams J and Ridgway M C 2016 Porosity as a function of stoichiometry and implantation temperature in $Ge/Si_{1-x}Ge_x$ alloys *J. Appl. Phys.* **119** 094303
[41] Romano L, Impellizzeri G, Bosco L, Ruffino F, Miritello M and Grimaldi M 2012 Nanoporosity induced by ion implantation in deposited amorphous Ge thin films *J. Appl. Phys.* **111** 113515
[42] Dell'Anna R, Iacob E, Barozzi M, Vanzetti L, Hübner R, Böttger R, Giubertoni D and Pepponi G 2018 The role of incidence angle in the morphology evolution of ge surfaces irradiated by medium-energy au ions *J. Phys. Condens. Matter* **30** 324001
[43] Yanagisawa J, Takarabe K, Ogushi K, Gamo K and Akasaka Y 2007 Nanoporous structure formations on germanium surfaces by focused ion beam irradiations *J. Phys.: Condens. Matter* **19** 445002
[44] Bradley R M and Shipman P D 2010 Spontaneous pattern formation induced by ion bombardment of binary compounds *Phys. Rev. Lett.* **105** 145501
[45] Böttger R, Bischoff L, Heinig K-H, Pilz W and Schmidt B 2012 From sponge to dot arrays on (100) ge by increasing the energy of ion impacts *Journal of Vacuum Science & Technology B, Nanotechnology and Microelectronics: Materials, Processing, Measurement, and Phenomena* **30** 06FF12
[46] Munoz-Garcia J, Vazquez L, Castro M, Gago R, Redondo-Cubero A, Moreno-Barrado A and Cuerno R 2014 Self-organized nanopatterning of silicon surfaces by ion beam sputtering *Materials Science and Engineering: R: Reports* **86** 1
[47] Anzenberg E, Perkinson J C, Madi C S, Aziz M J and Ludwig K F Jr 2012 Nanoscale surface pattern formation kinetics on germanium irradiated by kr+ ions *Phys. Rev.* B **86** 245412
[48] Teichmann M, Lorbeer J, Ziberi B, Frost F and Rauschenbach B 2013 Pattern formation on ge by low energy ion beam erosion *New J. Phys.* **15** 103029
[49] Herminghaus S, Jacobs K, Mecke K, Bischof J, Fery A, Ibn-Elhaj M and Schlagowski S 1998 Spinodal dewetting in liquid crystal and liquid metal films *Science* **282** 916
[50] Repetto L, Šetina Batič B, Firpo G, Piano E and Valbusa U 2012 Ion induced spinodal dewetting of thin solid films *Appl. Phys. Lett.* **100** 223113
[51] Repetto L, Savio R L, Batič B Š, Firpo G, Angeli E and Valbusa U 2015 A liquid-like model for the morphology evolution of ion bombarded thin films *Nucl. Instrum. Methods Phys. Res.* B **354** 28
[52] Torquato S 1999 Exact conditions on physically realizable correlation functions of random media *J. Chem. Phys.* **111** 8832
[53] Wilken S, Guerra R E, Pine D J and Chaikin P M 2020 Hyperuniform structures formed by shearing colloidal suspensions *Phys. Rev. Lett.* **125** 148001
[54] Xie R, Long G G, Weigand S J, Moss S C, Carvalho T, Roorda S, Hejna M, Torquato S and Steinhardt P J 2013 Hyperuniformity in amorphous silicon based on the measurement of the infinite-wavelength limit of the structure factor *Proc. Natl. Acad. Sci. U.S.A.* **110** 13250
[55] Minkowski H 1989 Volumen und oberfläche *Ausgewählte Arbeiten zur Zahlentheorie und zur Geometrie* (Springer) pp 146–92
[56] Schneider R 2014 *Convex Bodies: The Brunn-Minkowski Theory* vol 151 (Cambridge University Press)
[57] Mantz H, Jacobs K and Mecke K 2008 Utilizing minkowski functionals for image analysis: a marching square algorithm *J. Stat. Mech.: Theory Exp.* **12** P12015
[58] Galinski H, Ambrosio A, Maddalena P, Schenker I, Spolenak R and Capasso F 2014 Instability-induced pattern formation of photoactivated functional polymers *Proc. Natl. Acad. Sci. U.S.A.* **111** 17017
[59] Alkemade P 2006 Propulsion of ripples on glass by ion bombardment *Phys. Rev. Lett.* **96** 107602
[60] Norris S A and Aziz M J 2019 Ion-induced nanopatterning of silicon: toward a predictive model *Applied Physics Reviews* **6** 011311
[61] Herminghaus S, Jacobs K, Mecke K, Bischof J, Fery A, Ibn-Elhaj M and Schlagowski S 1998 Spinodal dewetting in liquid crystal and liquid metal films *Science* **282** 916
[62] Galinski H, Fratalocchi A, Döbeli M and Capasso F 2017 Light manipulation in metallic nanowire networks with functional connectivity *Adv. Opt. Mater.* **5** 1600580
[63] Galinski H, Favraud G, Dong H, Gongora J S T, Favaro G, Döbeli M, Spolenak R, Fratalocchi A and Capasso F 2017 Scalable, ultra-resistant structural colors based on network metamaterials *Light Sci. Appl.* **6** e16233
[64] Chowdhury D, Mondal S, Secchi M, Giordano M C, Vanzetti L, Barozzi M, Bersani M, Giubertoni D and de Mongeot F B 2022 Omnidirectional and broadband photon harvesting in self-organized ge columnar nanovoids *Nanotechnology* **33** 305304
[65] Tavakoli N *et al* 2022 Over 65 sunlight absorption in a 1 μm si slab with hyperuniform texture *ACS Photonics* **9** 1206
[66] Soukoulis C M and Wegener M 2011 Past achievements and future challenges in the development of three-dimensional photonic metamaterials *Nat. Photonics* **5** 523